Journal of Engineering and Applied Sciences 13 (Special Issue 2): 2978-2985, 2018
ISSN: 1816-949X

Study on the Flow Characteristics of the Urea-SCR Swirl Injector Using the Unsteady CFD Technique

[1]Eun-Jo Gwak and [2]Sung-Young Park
[1]Department of Mechanical Engineering, Graduate School,
[2]Division of Mechanical and Automotive Engineering, Kongju National University,
275 Budae-dong, Cheonan-si, 31080 Chungcheongnam-do, Korea

Abstract: The flow rate and swirl characteristics of the injector for the urea-SCR that are varied according to design changes were examined through an unsteady-flow analysis. The design parameters that were taken into account for the improvement of the intra-injector flow characteristics are the number of swirl passages, the nozzle-curvature radius and the length of the needle-end shape. The characteristics of the internal-flow rate were analyzed and the amount of the single-injection flow rate of the injector appeared to increase in accordance with the increasing of the number of swirl passages, the increasing of the nozzle-curvature radius and the decreasing of the length of the needle-end shape. The corresponding swirl characteristics were also analyzed and the swirl-disk-created rotary flow affected the outlet flow with a continuous increasing of the swirl coefficient until the termination of the injection. The average swirl-coefficient values were compared and the results indicate that a lesser number of swirl passages, a bigger nozzle-curvature radius and a longer needle-end shape are advantageous for the enhancement of the swirl intensity. The analysis of the urea-SCR injector that was conducted in this study is likely to be exploited as a basic study for the design and performance enhancements of single-swirl injectors.

Key words: CFD, internal flow characteristics, overset mesh, swirl coefficient, urea-SCR injector, analysis

INTRODUCTION

To cope with the increasing global environmental regulations that have resulted from global warming and the depletion of fossil fuels, the automobile industry is currently carrying out diverse studies for the development of environmentally friendly "green cars" that are capable of reducing the harmful exhaust emissions through the realization of an excellent energy-consumption efficiency. As a part of the studies, the new diesel engines with reduced emissions of harmful exhausts and increased mileages that have been realized through the application of new technologies such as CRDI (Common Rail Direct Injection) and VGT (Variable Geometry Turbocharger) are under the spotlight. Diesel engines which generally show a higher energy consumption efficiency and compression ratio than the ordinary spark-ignition engines are currently mounted on commercial vehicles, SUVs and even in passenger cars (Snow *et al*., 2007; Ham and Park, 2011; Jeong *et al*., 2011).

The harmful diesel-engine emissions of particulate matters and Nitrogen Oxides (NO_x), however have been known to exceed the levels of gasoline engines (Girard *et al*., 2007). The emission of harmful NOx from a diesel engine can be reduced through post-processing systems such as LNT (Lean NOx Traps), LNC (Lean NOx Catalysts) and SCR (Selective Catalytic Reduction) systems (Gwak and Park, 2016). The urea-SCR system is currently applied to actual commercial engines owing to its high NO_x-conversion efficiency and due to the intensifying regulation of exhausts, its gradual application to passenger cars is expected (Colombo *et al*., 2012; Koebel *et al*., 2000). For the application of urea-SCR system to vehicles, the completion of preceding studies on the performance of the urea injector are required. Figure 1 shows the overall arrangement of the post-processing scheme of a diesel engine where in the position of the urea-SCR system is illustrated. The performance of the urea injector which is an essential component of the dosing system isknown for its dominant effect on the reduction of NO_x (Han *et al*., 2010; Ham *et al*., 2009; Kim *et al*., 2006).

Han and Kim *et al*. have carried out a study on the position and shape of the urea injector, the injection

Corresponding Author: Sung-Young Park, Division of Mechanical and Automotive Engineering, Kongju National University, 275 Budae-dong, Cheonan-si, 31080 Chungcheongnam-do, Korea

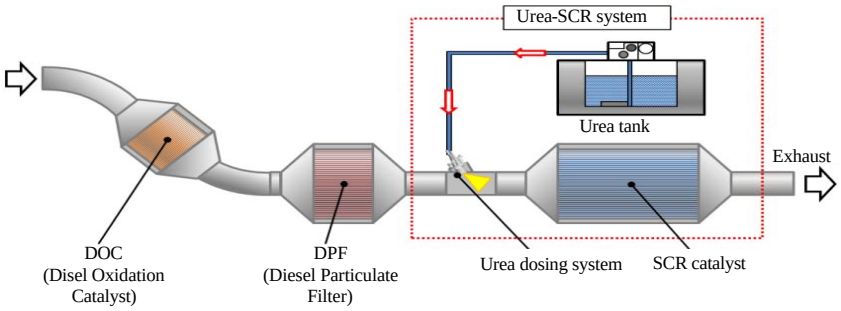

Fig. 1: Schematic diagram of exhaust-treatment system

pressure and the shape of the inlet to the SCR catalyst through the conduction of a spray-visualization test (Kowatari *et al*., 2006; Seo *et al*., 2008). However, the studies that are intended for the design and performance enhancements through an examination of the internal-flow characteristics of the injectors are yet to be furthered. Lee and Park (2014) have conducted an analytical study on the internal flow of injectors for the design purpose wherein the varied flow characteristics from the changed internal shape of the swirl injector for urea-SCR were identified and the correlation between the internal shape of the injector and the injection characteristics was analyzed through an unsteady-flow analysis to secure basic data for the development of new injectors.

MATERIALS AND METHODS

3D-modeling of an injector

Reverse engineering: To obtain the design data of the internal structure of a urea-SCR injector, reverse engineering was carried out on the urea-SCR injector that is applied in commercial vehicles. The internal structure of the injector employed in this study was secured through precision grinding and the corresponding 3-Dimensional (3D) modeling was carried out using the reverse-engineering approach. Figure 2 shows the cut-injector model and the 3D Model that was prepared through reverse engineering.

The injector used in this study was supplied from "B" company and is a single-hole swirl injector equipped with an outlet with a diameter of 250 μm. The injector was also equipped with an internal swirl disk that creates the injection-flow swirl. The nozzle direction deviates 20° from the direction of the intra-injector flow. Figure 3 shows the shapes of the injector-nozzle area, the region of interest and the swirl disk of the 3D Model.

Selection of the injector-design parameters: The design parameters that were applied to the swirl injector for the

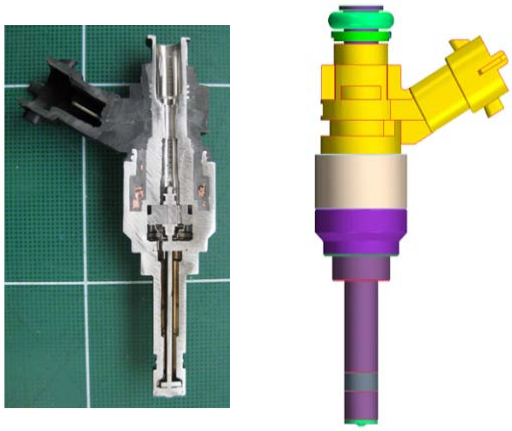

Fig. 2: Urea injector and generated 3D Model

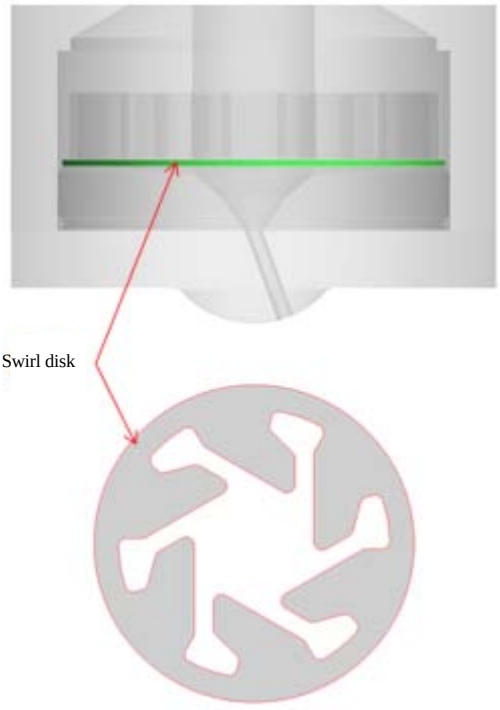

Fig. 3: Shape of the injector nozzle and swirl disk

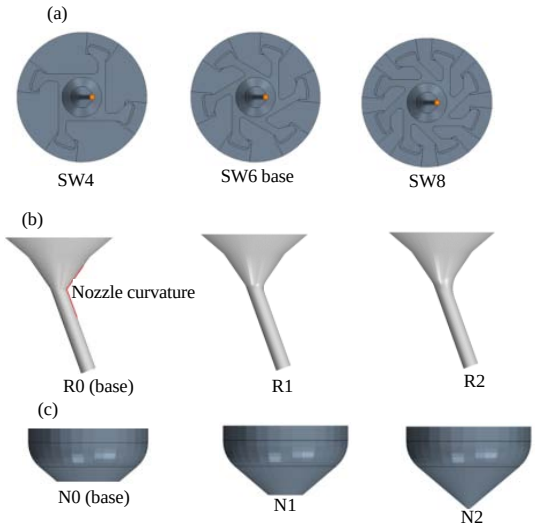

Fig. 4: Design parameters of the injector: a) Swirl disk; b) Radius of the nozzle curvature and c) Needle-end shape

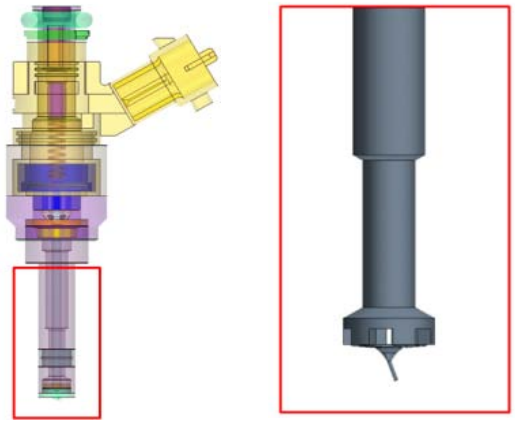

Fig. 5: Injector model and simulation domain

urea-SCR that was used in this study are the number of swirl passages, nozzle-curvature radius and of needle-end-shape length. The standards of the design parameters are presented in Fig. 4. The modification of each model that is based on the base SW6-R0-N0 Model is summarized in Table 1 and the shapes that resulted from the application of the design parameters are illustrated in Fig. 4.

Analytical methods

Meshes for the intra-injector flow computation: The 3D injector Model employed in this study is illustrated in Fig. 5a and the extraction of the corresponding flow domain is illustrated in Fig. 5b. In this study, since, the region of interest is the area around the nozzle including the swirl disk, the top of the injector was excluded from the simulation domain.

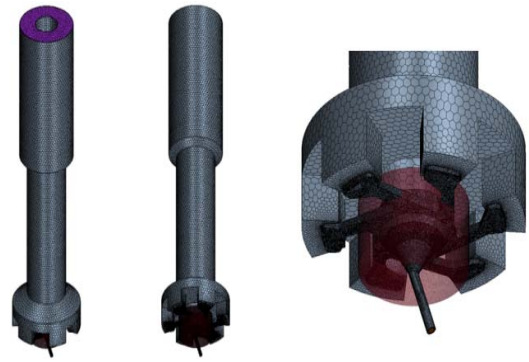

Fig. 6: Mesh of the simulation domain

Table 1: Design-parameter values

Models	Number of swirl passages	Radius of nozzle curvature (mm)	Needle-end shape (mm)
SW6-R0-N0 (Base model)	6	-	0.55
SW4-R0-N0	4	-	0.55
SW8-R0-N0	8	-	0.55
SW6-R1-N0	6	0.2	0.55
SW6-R2-N0	6	0.4	0.55
SW6-R0-N1	6	-	0.75
SW6-R0-N2	6	-	0.95

Table 2: Mesh setting for the internal-flow simulation

Region/Properties	Values
Fluid	
Mesh type	Polyhedral mesh
Base size (mm)	0.2
Number of prism layers (-)	5.00
Prism-layer thickness (mm)	0.03
Minimum surface size (mm)	0.02
Needle	
Mesh type	Polyhedral mesh
Base size (mm)	0.1
Number of prism layers (-)	5.00
Prism-layer thickness (mm)	0.03
Minimum surface size (mm)	0.01

The computational meshes that were prepared for the internal-flow analysis were created from the mesher provided in the Star-CCM+ and for the application of the overset-mesh technique, the fluid and external needle flow domains were distinguished (CD-Adapco, 2016). The settings for the meshes are summarized in Table 2 wherein approximately 1.50-1.80 million meshes were created according to each model. The meshes that were created for the computation of the SW6-R0-N0 Model, the base model are illustrated in Fig. 6.

Analytical conditions: For the computation of the intra-injector flow that is an unsteady turbulent flow the standard K-ϵ turbulence model was used. The five-prism-layer meshes were constructed and the inlet pressure to the injector was set as 0.7 MPa while that of the outlet to the nozzle is the barometric pressure. Since, the physical

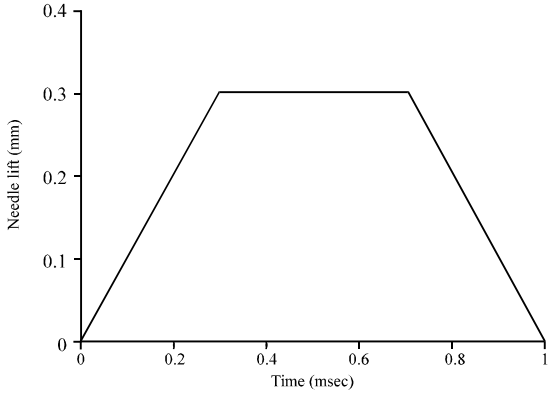

Fig. 7: Needle profile

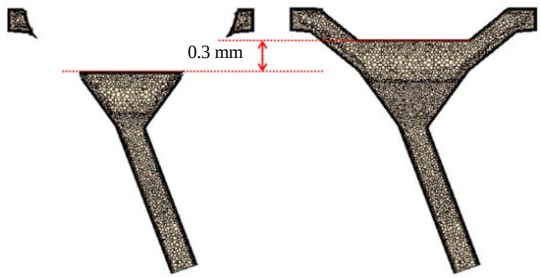

Fig. 8: Computational grid

characteristics of the urea solution are similar to those of water, the properties of water were set for the analyses that were conducted in this study (Lee and Park, 2014).

To simulate the movement of the needle, the lift profile of a needle was configured as illustrated in Fig. 7. It was therefore assumed that the needle rose for 0.3 msec, remaining at its peak lift for 0.4 msec and then fell down afterward for 0.3 msec. The speed of the rise and fall of the needle was assumed as constant for the analysis. The needle would rise by a maximum of 3 mm and the computational grids at the peak lift and the initial state are illustrated in Fig. 8.

RESULTS AND DISCUSSION

Mass-conservation law: The flow characteristics at the inlet and outlet of the base model were analyzed to identify the mass-conservation law. Figure 9 shows the flow characteristics and the difference in the flow rate that was varied over time at the inlet and outlet of the injector. In the analyses of this study, the analytical domain for the inside of the control volume was changed according to the movement of the needle and the difference in the flow rate at the inlet and outlet is equal to the mass change inside the control volume.

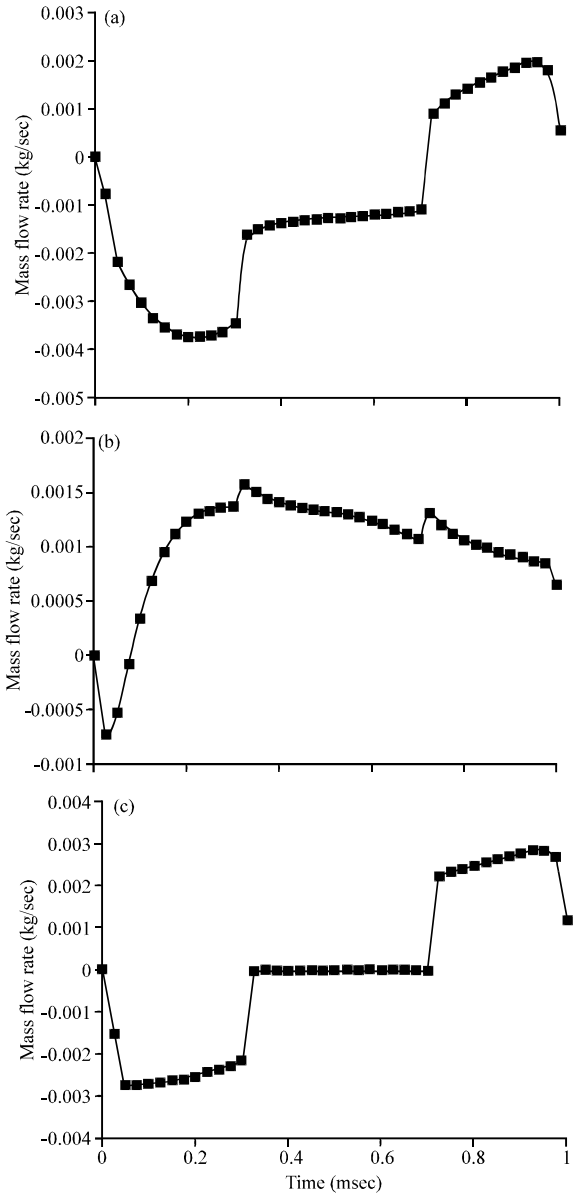

Fig. 9: Mass-flow-rate results (SW6-R0-N0): a) Inlet; b) Outlet and c) Difference between inlet and outlet

The mass-conservation law can be represented as the expression of Eq. 1. The amount of the mass change inside the control volume (Δm_{CV}) that was varied over time and the cumulative integration as well as the mass-change amount (Δm_{CS}) of the difference in the mass-flow rate Fig. 9c over time between the inlet and the outlet are illustrated in Fig. 10. The sum of the amounts of the two mass changes is $\Delta m_{CV}+\Delta m_{CS} = 0$ according to the mass-conservation law. The errors of the theoretical amount of the mass change inside the control volume and

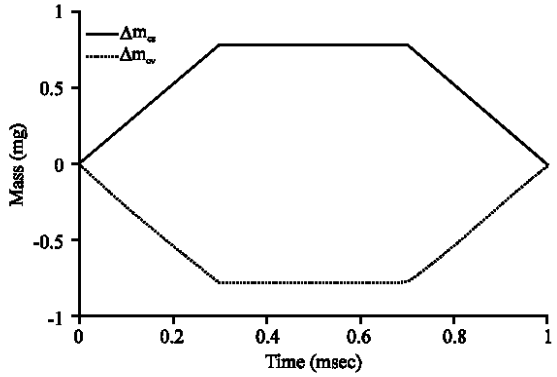

Fig. 10: Calculated mass conservation of the simulation

of that at the inlet and the outlet were identified as <1% and thereby comply with the mass-conservation law:

$$\frac{d}{dt}\int_{CV}\rho dV+\int_{CS}\rho\vec{V}.d\vec{A}=0 \quad (1)$$

Internal-flow characteristics: The flow rates at the outlet of each model are illustrated in Fig. 11. The results that were obtained by varying the number of swirl passages are illustrated in Fig. 11a whereas those that were obtained by varying the radius of the nozzle curvature and by varying the shape of the needle end are illustrated in Fig. 11b and c, respectively. The distributions of the intra-injector pressure and of the 0.5 msec speeds at the inlet and outlet of each model are summarized in Fig. 12 and 13 for the analysis of the internal-flow characteristics. The flow rate at the outlet increased in accordance with the increasing number of swirl passages Fig. 11a and the internal total pressure was increased as well Fig. 12. These observations are attributable to the internal-flow resistance that was decreased by the increasing number of swirl passages. Along with the increasing radius of the nozzle curvature, the vena contracta decreased Fig. 12 whereas the flow rate at the outlet increased accordingly Fig. 11b. In the case of the extended length of the needle-end shape (N1 or N2), the 0.5 msec post-injection flow rate at the outlet decreased compared with the base model Fig. 11c with the distribution of a low total pressure and the reduced speed at the outlet Fig. 12 and 13. The consequences were derived from the increased swirl intensity which is ascribable to the remaining rotary flow, until it reached the inlet to the nozzle Fig. 14. The increase of this swirl momentum decreased the momentum of the axial flow and resulted in the decreased flow rate of the outlet.

To compare the single-injection amounts, one of the major injector-performance factors, Eq. 2 was used for the calculation. This is an integration of the mass-flow rate

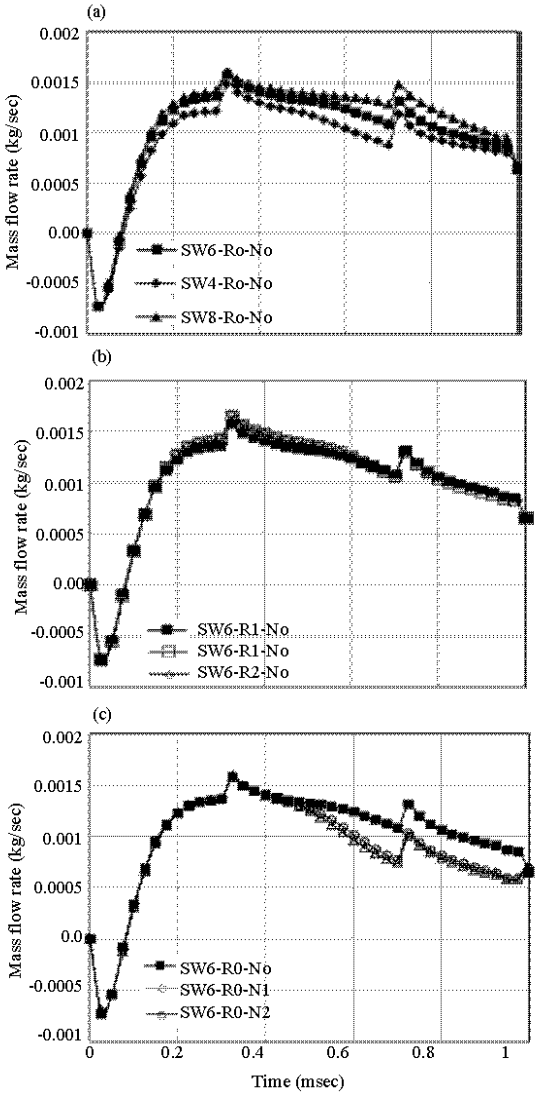

Fig. 11: Mass-flow rate on the outlet: a) Change of number of swirl passages; b) Change of nozzle-angle round and c) Change of needle-end-shape length

over time from the point of the initiation of the rise of the needle to the time point of 1ms after the termination of the injection as follows:

$$m_{total}=\int \dot{m}dt \quad (2)$$

The single-injection amounts of each model and the rates of the corresponding increase (or decrease) compared with those of the base model are summarized in Table 3. The single-injection amounts appeared to increase in accordance with the increasing number of swirl passages, the increasing radius of the nozzle curvature and the decreasing length of the shape of the needle end. The highest single-injection amount is from the

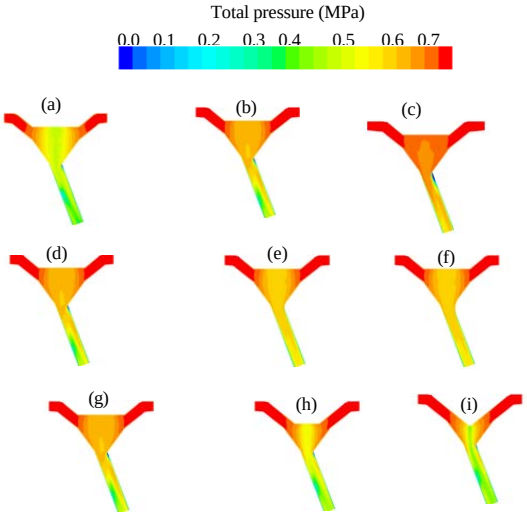

Fig. 12: Total pressure inside the nozzle (at 0.5 msec): a) SW4-R0-N0; b) SW6-R0-N0 (base); c) SW8-R0-N0; d) SW6-R0-N0 (base); e) SW6-R1-N0; f) SW6-R2-N0; g) SW6-R0-N0 (base); h) SW6-R0-N1 and i) SW6-R0-N1

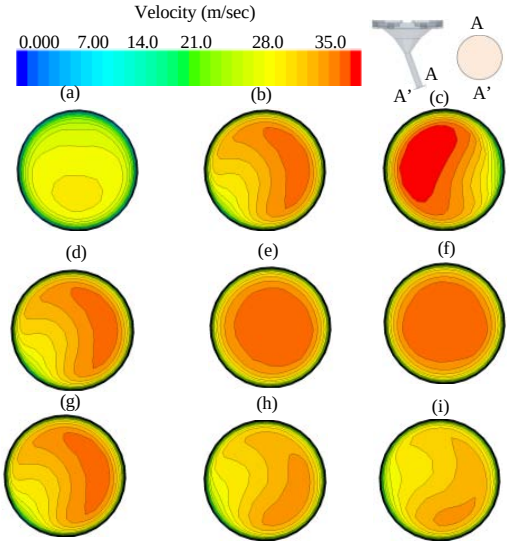

Fig. 13: Velocity field on the outlet (at 0.5 msec): a) SW4-R0-N0; b) SW6-R0-N0 (base); c) SW8-R0-N0; d) SW6-R0-N0 (base); e) SW6-R1-N0; f) SW6-R2-N0; g) SW6-R0-N0 (base); h) SW6-R1-N0 and i) SW6-R2-N0

Table 3: Injection quantity

Models	Total out mass (mg)	Rate of change (%)
SW6-R0-N0 (base)	1.0230	-
SW4-R0-N0	0.9046	- 13.08
SW8-R0-N0	1.1130	8.09
SW6-R1-N0	1.0396	1.59
SW6-R2-N0	1.0461	2.21
SW6-R0-N1	0.9116	- 12.22
SW6-R0-N2	0.8953	- 14.26

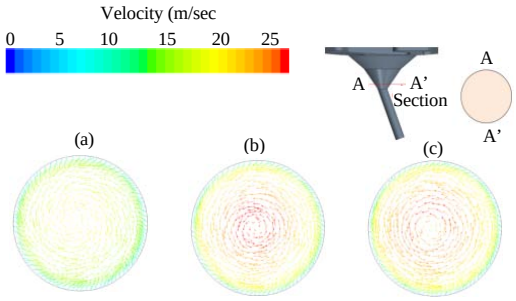

Fig. 14: Velocity vector according to the change of the needle-end-shape length (at 0.6 msec): a) SW6-R0-N0; b) SW6-R0-N1 and c) SW6-R0-N2

SW8-R0-N0 Model which was equipped with the largest number of swirl passages, resulting in an increase of approximately 8% compared with the base model. Besides, the SW6-R0-N2 Model that was furnished with the longest needle-end-shape length produced the lowest single-injection amounts that are approximately 14% smaller than those of the base model.

Swirl characteristics: The swirl coefficient denotes the ratio of the rotary-flow momentum to that of the axial flow. The swirl coefficient was calculated at the exit plane of the nozzle outlet using Eq. 3. In the equation, the U and α, respectively denote the magnitude in the tangential direction of an arbitrary vector on the exit plane and the angle to the central axis as follows:

$$C_{swirl} = \frac{\int U\alpha da}{\dot{m}} \quad (3)$$

The swirl-coefficient values of each model that were configured with the respective design parameters were plotted on the graph that is illustrated in Fig. 15 to analyze the respective swirl characteristics. The rotary-flow time that was created by the swirl disk affecting the outlet appeared after 0.3 msec while the value of the swirl coefficient increased continuously to the point of the termination of the injection that followed the falling down of the needle. Figure 16 shows the velocity vector on the exit plane at the time point of 0.7 msec. The vector was represented using the gray scale to identify the relative speed wherein the darker aspects signify the faster velocities. The higher values of the swirl coefficient appeared in correspondence with the fast flows near the nozzle wall.

To compare the respective swirl characteristics quantitatively, the values of the average swirl coefficient were calculated. The value of the average swirl coefficient resulted from the values of the swirl coefficient in the region from the time point of 0.3 msec where the needle

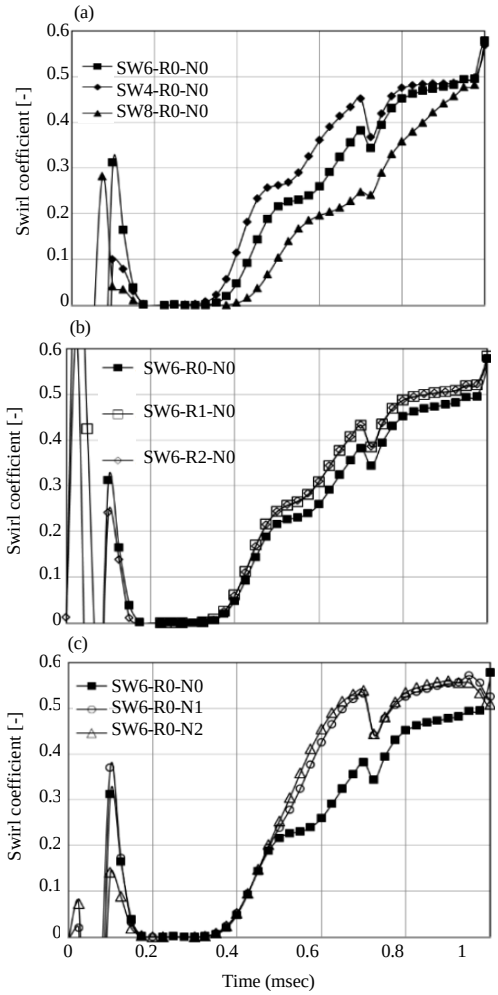

Fig. 15: Swirl-coefficient results

Table 4: Averaged swirl coefficients

Models	Averaged swirl coefficient (-)	Rate of change (%)
SW6-R0-N0 (Base)	0.2958	-
SW4-R0-N0	0.3534	16.30
SW8-R0-N0	0.2342	-26.30
SW6-R1-N0	0.3397	12.92
SW6-R2-N0	0.3402	13.05
SW6-R0-N1	0.3845	23.07
SW6-R0-N2	0.3928	24.69

reaches its peak lift to the time point of 1.0 msec of the termination of the injection. The rates of the increase or the decrease of the average swirl coefficient of each model compared with those of the base model are summarized in Table 4. Except for the SW8-R0-N0 Model that is equipped with eight swirl passages, the values of the average swirl coefficient of all of the other models appeared to increase. The SW6-R0-N2 Model with the longest needle-end-shape length represents the biggest swirl-coefficient value which is approximately 24% higher

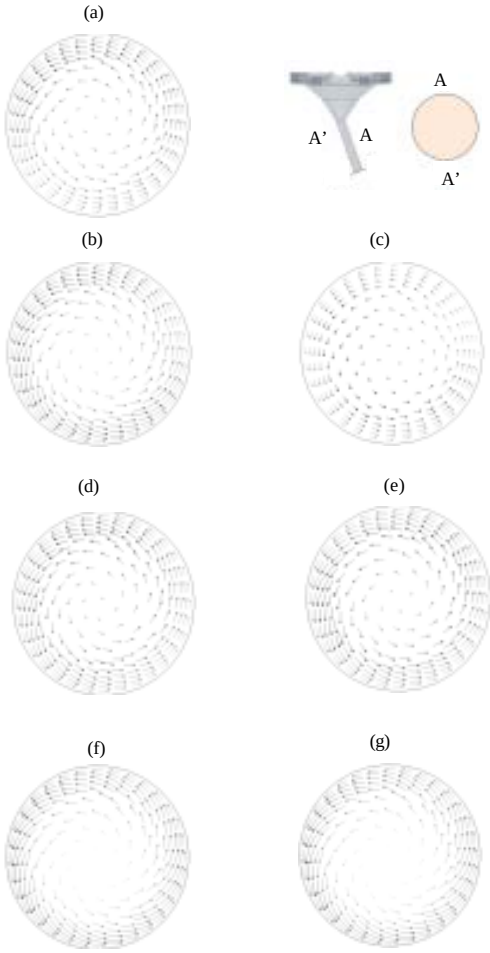

Fig. 16: Comparison of the velocity vectors on the outlet (at 0.7 msec): a)SW6-R0-N0 (base); b) SW4-R0-N0; c) SW8-R0-N0; d) SW6-R1-N0; e) SW6-R2-N0; f) SW6-R0-N1 and g) SW6-R0-N2

than that of the base model. The SW8-R0-N0 Model that produced the smallest average-swirl-coefficient value which comprises the largest number (eight) of swirl passages isattributable to the increased number of swirl passages that resulted in the reduction of the flow resistance and the axial flow became comparatively intensified in terms of the corresponding rotary-flow increase. It was finally concluded that a lesser number of swirl passages, a bigger nozzle-curvature radius and a longer needle-end shape are advantageous for the enhancement of the swirl intensity.

CONCLUSION

In this study, unsteady-flow analyses regarding the flow and swirl characteristics of the swirl injector for the urea-SCR were carried out through an exploitation of the

overset-mesh technique to identify the corresponding flow-rate and swirl characteristics that were varied according to the changes of the design parameters.

The reliability of the overset-mesh technique that was employed in this study was verified through the mass-conservation law with error rates that were calculated as <1%, showing the conformance of the results from all of the employed models. The flow-rate characteristics of the injector which were varied according to the changed design parameters were analyzed. The single-injection amount of the injector apparently increased in accordance with the increasing number of swirl passages, the increasing radius of the nozzle curvature and the decreasing length of the shape of the needle end. The SW8-R0-N0 Model which was equipped with the largest number of swirl passages, generated the biggest single-injection amount that is approximately 8% higher than that of the base model.

The swirl characteristics of the injector were examined and the rotary flow that is created by the swirl disk affected the outlet after a time point of 0.3 msec together with a continuous increasing of the swirl coefficient to the point of the termination of the injection. The values of the average swirl coefficient which were varied according to the changes in the design parameters of each model were also analyzed and the swirl intensity increased along with the lessening of the number of swirl passages, the increasing of the radius of the nozzle curvature and the lengthening of the needle-end shape.

It is expected that the results that were obtained from the swirl-injector analyses for the urea-SCR that were conducted in this study will be used as basic information in the performance-enhancement and design-work practices regarding the swirl injectors for the urea-SCR.

REFERENCES

CD-Adapco, 2016. Star-CCM+ ver. 11.04 user guide. CD-Adapco, Melville, New York, USA.

Colombo, M., I. Nova, E. Tronconi, V. Schmeiber and B. Bandl-Konrad *et al.*, 2012. 2012. NO-NO_2/N_2 O-NH_3 SCR reactions over a commercial Fe-zeolite catalyst for diesel exhaust aftertreatment: Intrinsic kinetics and monolith converter modelling. Appl. Catal. B. Environ., 111: 106-118.

Girard, J., R. Snow, G. Cavataio and C. Lambert, 2007. The Influence of Ammonia to NOx ratio on SCR Performance. SAE International, Michigan.

Gwak, E.J. and S.Y. Park, 2016. Study on the flow characteristics of Urea-SCR swirl injector according to the needle lift profile. J. Korea Acad. Ind. Cooperation Soc., 17: 650-655.

Ham, Y.Y. and Y.S. Park, 2011. Development of map based open loop control algorithm for urea-SCR system. Trans. Korean Soc. Automot. Eng., 19: 50-56.

Ham, Y.Y., S.W. Kim and H.S. Jung, 2009. A study on the effect of the air-assist injection nozzle configurations on DeNOx characteristics in Urea-SCR system. Trans. Korean Soc. Automot. Eng., 17: 67-73.

Han, J.W., H.J. Gong, I.G. Hwang, C.L. Myung and S.S. Park, 2010. Experimental investigation on DeNOx performance according to the Urea-SCR system control at various operating conditions for diesel engines. Trans. Korean Soc. Automot. Eng., 18: 76-83.

Jeong, S.J., W.S. Kim, J.K. Park, H.K. Lee and S.D. Oh, 2011. The development and implementation of model-based control algorithm of urea-SCR dosing system for improving De-NOx performance and reducing NH3-slip. Proceedings of the ASME-JSME-KSME 2011 Joint Conference on Fluids Engineering, July 24-29, 2011, ASME, Hamamatsu, Japan, ISBN:978-0-7918-4440-3, pp: 905-913.

Kim, K.D., W.H. Youn, B.S. Kim, J.S. Ha and K.H. Ahn *et al.*, 2006. Performance simulation for the variation of fuel injection nozzle configurations in medium speed diesel engine. J. Korean Soc. Mar. Eng., 30: 662-668.

Koebel, M., M. Elsener and M. Kleemann, 2000. Urea-SCR: A promising technique to reduce NOx emissions from automotive diesel engines. Catal. Today, 59: 335-345.

Kowatari, T., Y. Hamada, K. Amou, I. Hamada and H. Funabashi *et al.*, 2006. A study of a new aftertreatment system 1: A new dosing device for enhancing low temperature performance of urea-SCR. SAE International, Michigan.

Lee, S.I. and S.Y. Park, 2014. Numerical analysis of internal flow characteristics of urea injectors for SCR dosing system. Fuel, 129: 54-60.

Seo, J.W., K.I. Lee, J.T. Oh, Y.H. Choi and J.H. Lee *et al.*, 2008. The study on the effects of mixer configurations on fluid mixing characteristics in SCR systems. Trans. Korean Soc. Automot. Eng., 16: 192-199.

Snow, R., G. Cavatatio, D. Dobson, C. Montreuil and R. Hammerle, 2007. Calibration of a LNT-SCR Diesel Aftertreatment System. SAE International, Michigan.